International Journal of Thermal Sciences 48 (2009) 1327–1337

Contents lists available at ScienceDirect

International Journal of Thermal Sciences

www.elsevier.com/locate/ijts

An integral approach for simulation of vapour film dynamics around a spherical surface

Koushik Ghosh *, Achintya Mukhopadhyay, Swarnendu Sen, Dipankar Sanyal

Department of Mechanical Engineering, Jadavpur University, Kolkata 700 032, India

ARTICLE INFO

Article history:
Received 3 September 2007
Received in revised form 29 April 2008
Accepted 20 November 2008
Available online 19 December 2008

Keywords:
Integral model
ODE
Film dynamics
Variable density
Scale analysis
Bubble growth
Bubble collapse

ABSTRACT

The dynamics of a thermally driven vapour film around a solid sphere has been investigated here with both the sphere and the annular film surrounded by a large water pool. Integral models based on constant and variable vapour-phase densities have been developed here for studying a spherico-symmetric phase change problem for two immiscible phases, vapour and liquid around a hot sphere. Governing equations for both liquid and vapour phases are converted into a set of non-linear ODEs. Effects of distinct density on interface condition and density variation of vapour phase are taken into account both in energy equation of vapour phase and also in interfacial mass and energy balance. The present models have been validated with available analytical, incompressible Volume of Fluid (VOF) and experimental results of growth and collapse of either bubble or vapour film. A simple model, based on scale analysis, was evolved that successfully captured the non-monotonic growth of the film, as observed by the more detailed models under certain degree of liquid subcooling. In addition, the case of very small thermal boundary layer in the liquid side has been successfully studied for which the VOF model required very fine grid. It has been observed that the effect of density variation in the integral model results in marginally higher film growth at higher temperature. However, the effect of radiation on the film growth was found to be quite substantial. The integral model not only incorporates the effects of vapour-phase temperature variation and radiation exchange of heat but also is computationally several-fold efficient with respect to the VOF model.

© 2008 Elsevier Masson SAS. All rights reserved.

1. Introduction

Two immiscible phases separated by an interface are present in many engineering problems involving phase change. If the phase interface between the liquid and its vapour is associated with sharp temperature gradient, evaporation and transport of mass take place across the interface causing it to move. Plesset and Zwick [1] investigated the inertia-controlled spherico-symmetric dynamics of a vapour bubble in a pool of water. Their prediction is reasonable during the initial period, if the liquid superheat is high or the system pressure is low. A perturbation analysis of the energy equation in presence of a thermal boundary layer in the liquid side revealed that towards the terminal phase the dynamics is thermally maintained. Mikic et al. [2] obtained a unified expression of the radius of a saturated vapour bubble combining the results of simple scale analyses for both the inertial and thermally controlled regimes. Their prediction exhibited good agreement with those of Dalle Donne and Ferranti [3], except for very small liquid superheats.

Prosperetti and Plesset [4] extended the solution of Mikic et al. [2] by introducing scaling variables to describe growth over a wide range of superheats. Lee and Merte [5] and Robinson and Judd [6] carried out detailed numerical analysis of spherico-symmetric bubble growth in superheated liquid. Naude and Mendez [7] numerically analysed the collapse of vapour bubble in subcooled liquid. Riznic et al. [8] assumed spherico-symmetry in order to carry out an integral analysis associated with a vapour bubble for its collapse in a subcooled liquid pool and growth in a superheated liquid pool. While Prosperetti and Plesset [4] and Robinson and Judd [6] included the inertial effect on thermal growth in their scale analysis, Naude and Mendez [7] and Riznic et al. [8] neglected the effect of liquid momentum to lay emphasis only on thermally driven growth and collapse. Avdeev and Zudin [9] extended the regime of applicability of the solution by Mikic et al. [2] by incorporating the effects of heat inflow and inertial reaction of the liquid to bubble expansion in the energy transport and Rayleigh equations for the bubble. Their approximate analytical solution captured the features of certain experimental findings for the first time. The solution exhibited smooth transition from one parametric regime to another along with asymptotic approaches to the limiting solutions.

Closed form solutions for the thermally induced dynamics have been obtained by neglecting the density difference between the

* Corresponding author. Tel.: +91 33 24146177; fax: +91 33 24146532.
E-mail address: kghosh@mech.jdvu.ac.in (K. Ghosh).

1290-0729/$ – see front matter © 2008 Elsevier Masson SAS. All rights reserved.
doi:10.1016/j.ijthermalsci.2008.11.017

Nomenclature

a_2	time varying constant	T	time ..... s
C_p	specific heat of fluid ..... J/kg K	u	transformed variable $T.r$ ..... K m
J	evaporative mass flux across interface ..... kg/m^2 s	*Greek letters*	
Ja	Jakob number, $Ja = \rho_l C_p \lvert(T_s - T_\infty)\rvert/\rho_{v_s} L$, dimensionless	v	velocity ..... m/s
L	latent heat of phase change ..... J/kg	ρ	density ..... kg/m^3
R	interface radius ..... m	λ	thermal conductivity ..... W/m K
R_0	initial interface radius ..... m	α	thermal diffusivity ..... m^2/s
R_g	gas constant ..... J/kg K	δ	liquid-side thermal boundary layer thickness ..... m
R_m	sphere/melt radius ..... m	η	$(r - R_m)/(R - R_m)$, dimensionless
$\dot{R}$	interface velocity ..... m/s	ε	emissivity, dimensionless
Ste	Stefan number, $Ste = C_p(T_m - T_s)/L$, dimensionless	γ	surface tension co-efficient ..... N/m
T	temperature ..... K	σ	Stefan–Boltzmann constant ..... W/m^2 K^4
T_s	saturation temperature ..... K	*Subscripts*	
T_∞	far liquid temperature ..... K	l	liquid phase
h	enthalpy ..... J/kg	v	vapour phase
p	pressure ..... N/m^2	m	melt (sphere)
q_{rad}	radiation heat flux ..... W/m^2	s	saturation condition
R	radial co-ordinate ..... m		

phases for situations where a particular phase remains at saturation condition corresponding to the system pressure. These approximations lead to analytical solution in standard simple geometries that are known as solution to Stefan problem [10]. Application of Stefan problem is mainly pertinent to phase change in material storage device, where the interface movement arises from either melting or solidification of a particular phase. Caldwell and Kwan [11] solved the outward solidification problem for different geometries by perturbation methods.

If the phases are not saturated and, in addition, the difference in densities between two phases is considered, the problem differs from the Stefan-like situation. The interface boundary condition calls for the solution of energy equation in both phases with the bulk-phase motion activated by the motion of interface. In Cartesian geometry Carslaw and Jaeger [12] analysed the effect of difference in densities, with one phase at saturation temperature. For the validation of their code, both Welch and Wilson [13] and Esmaeeli and Tryggvasson [14] used the similarity solution for the outward movement of a planar liquid–vapour interface. In these formulations, the effect of distinct densities is crucial and convection of energy in the superheated bulk liquid is explicitly accounted for. However, the vapour phase was considered as saturated.

Another situation demands attention when the vapour film is between a molten metal in the interior and liquid at the exterior. Though such dynamic studies are of interest for the prediction of rapid collapse of a vapour film during molten fuel-coolant-interaction [15,16] and a number of other technical applications [15], these remain limited till date. Bejan et al. [17] and Dan et al. [18] investigated the growth of a vapour film around a molten metal drop immersed in a saturated liquid. They considered radiative heat transfer between the metal drop and the water, considering the vapour layer to be non-participating. In addition, they considered the convective heat transfer due to the radial velocity field induced by temporal and spatial variation of vapour phase density. However, this convective effect was not considered in their estimation of evaporation rate through mass and energy balance at the interface. Ghosh et al. [19] adopted a generalised incompressible Volume of Fluid (VOF) based methodology for prediction of collapse and growth of a thin vapour film layer formed around a hot sphere immersed in a large liquid pool.

In the present work, an ODE-based spherico-symmetric approximate integral model has been developed that can predict the collapse and growth of a thin layer of a vapour film formed around a hot sphere immersed in a large liquid pool. The VOF-based methodology [19], developed earlier for a similar configuration is computationally intensive and is difficult to extend to multiple drops in a real system. Our present model can capture the case of distinct but constant density for each phase. An interesting prediction of initial decrease of film size followed by growth from the VOF-based investigation has been used to validate the present formulation, in absence of any experimental result. A scale analysis has been performed to predict the duration of the initial decay and compared with the prediction of the integral analysis. For a rigorous validation of the integral formulation, a few other problems have also been considered for which either of analytical, experimental and other numerical results are available.

In contrast to the VOF study [19], the integral study brings out the additional effects of the density variation and consequent velocity field in the vapour phase. Also following Bejan et al. [17], the contribution of radiation heat flux from the hot sphere to steam–water interface has been incorporated, assuming the vapour film to be non-participating. In addition, the effect of radial velocity field induced by density variation in the vapour phase has been included in the equation for mass and energy balance at the interface that yields the expression for evaporation rate. The developed model has been validated against some of the available analytical and numerical solution for moving boundaries with one of the phases at saturated condition. Studies have been carried out next considering none of the phases as saturated. A detailed parametric study of the dynamics of film around the hot sphere in a subcooled liquid has finally been investigated.

2. Mathematical model

In this section the system of equations have been derived using mass and energy conservation principles, the liquid–vapour interface condition and boundary conditions for the bulk liquid phase of infinite expanse and the vapour phase of the limited expanse. In the ensuing derivation, the liquid phase has been considered incompressible along with spherico-symmetric assumption for all primary variables. Two alternative formulations have been developed, one assuming constant density for the vapour phase and the

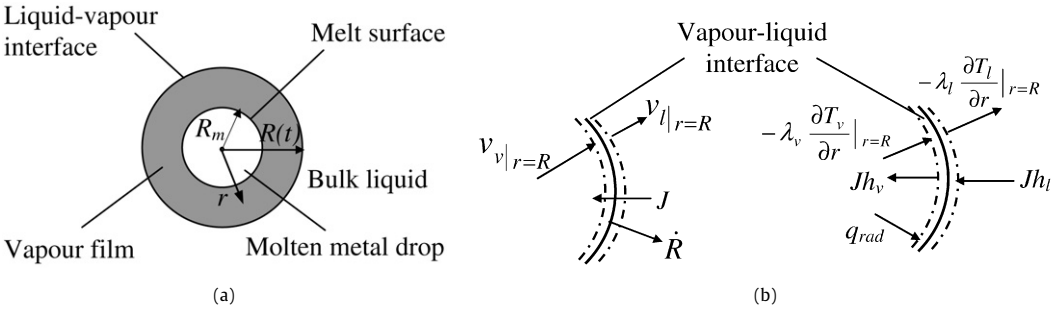

Fig. 1. Schematics of (a) computational geometry, (b) thermally-induced mass and energy transfer at the vapour–liquid interface.

other considering an isobaric density variation due to spatial and temporal variations in temperature.

For conservation of mass within the vapour phase shown in Fig. 1a, one can write

$$\frac{\partial \rho_v}{\partial t} + \frac{1}{r^2}\frac{\partial}{\partial r}\left(\rho_v r^2 v_v\right) = 0, \quad \text{for } R_m < r < R. \tag{2.1}$$

The principle of conservation of energy within the vapour phase can be expressed as

$$\frac{\partial}{\partial t}(\rho_v C_p T_v) + \frac{1}{r^2}\frac{\partial}{\partial r}\left(r^2 \rho_v C_p v_v T_v\right) = \frac{1}{r^2}\frac{\partial}{\partial r}\left(\lambda_v r^2 \frac{\partial T_v}{\partial r}\right), \quad \text{for } R_m < r < R. \tag{2.2}$$

Assuming constant property the above equation can be recast as

$$\frac{\partial T_v}{\partial t} + \frac{1}{r^2}\frac{\partial}{\partial r}\left(r^2 T_v v_v\right) = \frac{\alpha_v}{r^2}\frac{\partial}{\partial r}\left(r^2 \frac{\partial T_v}{\partial r}\right). \tag{2.3a}$$

Like earlier studies [17,18], the surface temperature of the sphere has been assumed constant in view of the timescale of interest in this work (~ 2 s) and the high thermal inertia of the sphere. In fact, detailed numerical simulation [19] revealed the temperature of the sphere to remain practically constant at its initial value. Bejan et al. [17] and Cacuci et al. [18] argued the inside the vapour, the changes of pressure and its associated saturation temperature to be small. Based on these observations, the conditions imposed at the sphere surface and the interface are as follows:

$$v_v|_{r=R_m} = 0, \tag{2.3b}$$

$$T_v|_{r=R_m} = T_m, \tag{2.3c}$$

$$T_v|_{r=R} = T_s. \tag{2.3d}$$

With reference to Fig. 1b, the flow continuity at the liquid–vapour interface yields

$$\rho_{v_s}(v_v|_{r=R} - \dot{R}) = \rho_l(v_l|_{r=R} - \dot{R}) = -J. \tag{2.4}$$

In the above equation, $\dot{R}$ denotes the rate of movement of the interface.

With reference to Fig. 1b, the energy balance across liquid and vapour interface can be expressed as

$$-Jh_v - \lambda_v \left.\frac{\partial T_v}{\partial r}\right|_{r=R} + q_{\text{rad}} = -Jh_l - \lambda_l \left.\frac{\partial T_l}{\partial r}\right|_{r=R}. \tag{2.5a}$$

This can be rearranged as

$$JL = -\lambda_v \left.\frac{\partial T_v}{\partial r}\right|_{r=R} + q_{\text{rad}} + \lambda_l \left.\frac{\partial T_l}{\partial r}\right|_{r=R}, \tag{2.5b}$$

where

$$L = h_v - h_l. \tag{2.5c}$$

The first and the second terms in the right-hand side of Eq. (2.5a), respectively, denote the conductive and radiative fluxes of heat into the vapour interface, while the last term corresponds to the conductive heat flux from the interface to the liquid side.

The continuity equation for incompressible bulk liquid domain is written as

$$\frac{\partial}{\partial r}\left(r^2 v_r\right) = 0. \tag{2.6}$$

Assuming constant property, the energy equation for the bulk liquid domain can be written in conservative form as

$$\frac{\partial T_l}{\partial t} + \frac{1}{r^2}\frac{\partial}{\partial r}\left(r^2 v_l T_l\right) = \frac{\alpha_l}{r^2}\frac{\partial}{\partial r}\left(r^2 \frac{\partial T_l}{\partial r}\right), \quad \text{for } R < r < \infty. \tag{2.7}$$

Assuming a thermal boundary layer thickness δ extending from the liquid–vapour interface at R into the liquid side and three boundary conditions at R and $R+\delta$ given as

$$T_l|_{r=R+\delta} = T_\infty, \tag{2.8a}$$

$$T_l|_{r=R} = T_s, \tag{2.8b}$$

$$\left.\frac{\partial T_l}{\partial r}\right|_{r=R+\delta} = 0 \tag{2.8c}$$

a quadratic temperature profile in the liquid domain can be obtained as

$$T_l = T_\infty + (T_s - T_\infty)\left(1 - \frac{r-R}{\delta}\right)^2. \tag{2.8d}$$

Now inserting Eq. (2.8d) in Eq. (2.7) and integrating the resulting expression from R to $R+\delta$, with the help of Leibnitz integral rule associated to a function $f(r,t)$ between limits $a(t) \leqslant r \leqslant b(t)$ given by

$$\frac{\partial}{\partial t}\int_{a(t)}^{b(t)} f(r,t)\,dr = \int_{a(t)}^{b(t)} \frac{\partial f(r,t)}{\partial t}\,dr + f(b,t)\frac{\partial b}{\partial t} - f(a,t)\frac{\partial a}{\partial t}, \tag{2.9}$$

along with using Eqs. (2.4) and (2.6), the energy equation in liquid domain is obtained as

$$\left\{\frac{1}{3} + \frac{1}{3}\left(\frac{\delta}{R}\right) + \frac{1}{10}\left(\frac{\delta}{R}\right)^2\right\}\dot{\delta} + \left\{\frac{2}{3}\left(\frac{\delta}{R}\right) + \frac{1}{6}\left(\frac{\delta}{R}\right)^2\right\}\dot{R} + \frac{J}{\rho_l} = \frac{2\alpha_l}{\delta}. \tag{2.10}$$

In the above equation, the symbol "·" denotes time derivative.

2.1. Constant density model

Applying Eq. (2.9) to expand the integral representing the rate of vapour accumulation within the film from the stationary melt

surface at $r = R_m$ with $\dot{R}_m = 0$ to the phase transforming liquid–vapour interface at $r = R$ with $\dot{R} \neq 0$, it can be written that

$$\frac{d}{dt}\int_{R_m}^{R} r^2 \rho_v \, dr = \int_{R_m}^{R} \frac{\partial}{\partial t}\left(r^2 \rho_v\right) dr + R^2 \rho_{v_s} \dot{R}.$$

Under the assumption of constant vapour density, the non-zero component of the accumulation term in the left-hand side of the above equation solely arises as a result of $\dot{R} \neq 0$. In addition, using Eq. (2.1) for the integrand on the right-hand side one obtains from the above equation that

$$v_v|_{r=R} = 0. \tag{2.11}$$

Eq. (2.4) together with the last equation provide the mass flux across the interface as

$$J = \rho_{v_s} \dot{R}. \tag{2.12}$$

Substituting J in Eq. (2.10), it is found that

$$\left\{\frac{1}{3} + \frac{1}{3}\left(\frac{\delta}{R}\right) + \frac{1}{10}\left(\frac{\delta}{R}\right)^2\right\}\dot{\delta} + \left\{\frac{2}{3}\left(\frac{\delta}{R}\right) + \frac{1}{6}\left(\frac{\delta}{R}\right)^2 + \frac{\rho_{v_s}}{\rho_l}\right\}\dot{R} = \frac{2\alpha_l}{\delta}. \tag{2.13}$$

As the density within the vapour film is assumed constant and the motion is neglected, Eq. (2.3a) can be rewritten in the equivalent Cartesian form as

$$\frac{\partial u}{\partial t} = \alpha_v \frac{\partial^2 u}{\partial r^2}, \tag{2.14a}$$

where the curvature effect of the spherical system is implicitly taken care of through the transformed variable

$$u = T_v r. \tag{2.14b}$$

Besides the transience within the constant-density vapour phase through accumulation of thermal energy, further non-linearity in the transformed variable could be envisaged with the movement of the phase-transforming boundary $r = R$. Moreover, the difference in heat transfer mechanisms at the two boundaries of the vapour phase calls for different instantaneous gradient of temperature that is attainable only by a non-linear profile. At $r = R_m$ the heat-flux boundary condition involves only diffusion, whereas at $r = R$ the boundary condition involves phase change as well. The simplest non-linear profile for the transformed variable in Eq. (2.14b) is of course quadratic. Assuming a quadratic profile for u in the form

$$u = a_0 + a_1\eta + a_2\eta^2, \tag{2.15a}$$

where a_0, a_1 and a_2 could be time-dependent coefficients and

$$\eta = (r - R_m)/(R - R_m). \tag{2.15b}$$

Using

$$u|_{\eta=0} = u_m \tag{2.15c}$$

and

$$u|_{\eta=1} = u_s \tag{2.15d}$$

in Eq. (2.15a), it is obtained that

$$u = u_m + (u_s - u_m - a_2)\eta + a_2\eta^2. \tag{2.15e}$$

Finally, using the variable of Eq. (2.14b) as the function f in the right-hand side of Eq. (2.9) and using Eq. (2.14a) for integrating the temporal derivative in terms of the spatial derivative within the vapour film, it is obtained by employing Eqs. (2.15b) and (2.15e) that

$$\left[3R_m(T_m - T_s) - a_2\right]\dot{R} - (R - R_m)\dot{a}_2 = \frac{12\alpha_v a_2}{(R - R_m)}. \tag{2.16}$$

Eq. (2.9) and the paired Eqs. (2.15b) and (2.15e) can be used to express the conductive heat flux terms in Eq. (2.5b). An expression for the radiative heat flux term in Eq. (2.5b) can be obtained by employing Stefan–Boltzmann equation along with the assumption that assuming both the metal surface and the liquid interface as gray diffuse and the intervening steam layer as transparent [17,18]. Following these manipulations in Eq. (2.5b) along with substitutions of Eqs. (2.5c) and (2.12), it can be obtained that

$$\rho_{v_s} L\dot{R} = \lambda_v \frac{R_m(T_m - T_s) - a_2}{R(R - R_m)} + \frac{\sigma R_m^2 (T_m^4 - T_s^4)}{\frac{R^2}{\varepsilon_m} + R_m^2\left(\frac{1-\varepsilon_l}{\varepsilon_l}\right)} - \frac{2\lambda_l(T_s - T_\infty)}{\delta}. \tag{2.17}$$

2.2. Scale analysis

A scale analysis often provides a simpler but gross estimation of certain quantities, which otherwise can be evaluated through obtaining a rigorous solution of the more complete mathematical description. In the context of dynamics of the film around the melt sustained by evaporation of the bulk liquid, such a scale analysis has been presented here for estimating the decaying time of the film prior to its initiation of growth. This time has been referred here as the rebound time.

The scale analysis pertains to the constant-property model. It is further assumed that the transport properties, temperatures of the melt and the bulk liquid along with the initial values of vapour film and liquid boundary layer are such that at the initial stage the conduction heat flux on the liquid side is much higher than both the conduction heat flux on the vapour side and radiative heat flux. Under the circumstances, Eq. (2.5b) together with Eq. (2.12) provide

$$\rho_{v_s}\dot{R}L \sim -\frac{\lambda_l(T_s - T_\infty)}{\delta(t)}. \tag{2.18}$$

In the above relation, the scale of T in the liquid layer is $(T_s - T_\infty)$ and the scale of radial distance is δ.

Neglecting initial thermal layer thickness on the liquid side, the scale of δ for the thermal penetration distance is obtained as

$$\delta \sim (\alpha_l t)^{1/2}. \tag{2.19}$$

Substituting the above expression of δ in Eq. (2.18), it is easy to find that

$$\dot{R} \sim -\frac{\lambda_l(T_s - T_\infty)}{L\rho_{v_s}(\alpha_l t)^{1/2}}. \tag{2.20}$$

Hence, the order of variation of film radius is estimated following the integration of the above equation as

$$R = R_0 - Ja(\alpha_l t)^{1/2}, \tag{2.21}$$

where Ja is Jakob number, defined as

$$Ja = \frac{\rho_l C_p |(T_s - T_\infty)|}{\rho_v L}. \tag{2.22}$$

Following the initial period of collapse of the film, the growth begins when the energy transport to the liquid–vapour interface through diffusion from inside of the vapour film and to the bulk liquid are of the same order. Beyond this time, already referred as the rebound time, the scale analysis is not expected to capture the qualitative trend of the growth dynamics in the correct manner.

Thus, the duration of validity of the scale analysis, or the order of rebound time predicted by the scale analysis, can be obtained by writing

$$\lambda_v \frac{\partial T_v}{\partial r}\bigg|_{r=R_m} \sim \lambda_l \frac{\partial T_l}{\partial r}\bigg|_{r=R_m}. \tag{2.23}$$

Taking the scale of temperature in vapour film side as $(T_m - T_s)$ and the scale of distance as $(R - R_m)$, it is obtained that

$$\frac{\lambda_v (T_m - T_s)}{(R - R_m)} \sim \frac{\lambda_l (T_s - T_\infty)}{\delta}. \tag{2.24}$$

Substituting Eq. (2.21) in the above expression, it is obtained that

$$\frac{\lambda_v (T_m - T_s)}{(R_0 - R_m - Ja(\alpha_l t)^{1/2})} \sim \frac{\lambda_l (T_s - T_\infty)}{(\alpha_l t)^{1/2}}. \tag{2.25}$$

Equating the both sides of the above approximate equation, the rebound time can be estimated as

$$t_{\text{rebound}} \sim (R_0 - R_m)^2 \Big/ \left(\frac{Ste}{Ja} \cdot \frac{\alpha_v}{(\alpha_l)^{1/2}} + Ja(\alpha_l)^{1/2} \right)^2, \tag{2.26a}$$

where Stefan number is defined as

$$Ste = C_p (T_m - T_s)/L. \tag{2.26b}$$

2.3. Variable density model

The continuity and energy equations in the vapour film in conservative form are

$$\frac{\partial \rho_v}{\partial t} + \frac{1}{r^2}\frac{\partial}{\partial r}\left(r^2 \rho_v v_v\right) = 0, \tag{2.27}$$

$$\frac{\partial}{\partial t}(\rho_v C_p T_v) + \frac{1}{r^2}\frac{\partial}{\partial r}\left(r^2 \rho_v C_p v_v T_v\right) = \frac{1}{r^2}\frac{\partial}{\partial r}\left(\lambda_v r^2 \frac{\partial T_v}{\partial r}\right). \tag{2.28}$$

Expanding Eq. (2.28) and using Eq. (2.27), it is possible to write

$$\rho_v C_p \left(\frac{\partial T_v}{\partial t} + v_v \frac{\partial T_v}{\partial r} \right) = \frac{1}{r^2}\frac{\partial}{\partial r}\left(\lambda_v r^2 \frac{\partial T_v}{\partial r}\right). \tag{2.29}$$

Although steam cannot be strictly modeled as an ideal gas, Craciunescu et al. [20] have demonstrated that ideal gas relations can be applied for modeling the interaction of even liquid water at supercritical pressures with reasonable accuracy. Assuming the vapour film to behave as an ideal gas, Eq. (2.29) can be expressed as

$$\frac{r^2}{T_v}\left(\frac{\partial T_v}{\partial t} + v_v \frac{\partial T_v}{\partial r} \right) = \frac{R_g}{pC_p}\frac{\partial}{\partial r}\left(\lambda_v r^2 \frac{\partial T_v}{\partial r}\right). \tag{2.30}$$

Expanding Eq. (2.27) and replacing the density term in Eq. (2.27) by $p/R_g T_v$, it is obtained that

$$\frac{r^2}{T_v}\left(\frac{\partial T_v}{\partial t} + v_v \frac{\partial T_v}{\partial r} \right) = \frac{\partial}{\partial r}\left(\lambda_v r^2 \frac{\partial T_v}{\partial r}\right). \tag{2.31}$$

Eqs. (2.30) together with (2.31) yield

$$\frac{\partial}{\partial r}\left(r^2 v_v\right) = \frac{R_g}{pC_p}\frac{\partial}{\partial r}\left(\lambda_v r^2 \frac{\partial T_v}{\partial r}\right). \tag{2.32}$$

Integrating the above equation from R_m to R, it is obtained that

$$R^2 v_v|_{r=R} = \frac{R_g}{pC_p}\left(\lambda_v R^2 \frac{\partial T_v}{\partial r}\bigg|_{r=R} - \lambda_v R_m^2 \frac{\partial T_v}{\partial r}\bigg|_{r=R_m} \right). \tag{2.33}$$

Evaluating the gradient from the temperature profile given by Eq. (2.15e), the above equation reduces to

$$v_v|_{r=R} = \frac{R_g}{pC_p R^2}\left(\lambda_v \frac{RR_m(T_s - T_m) + Ra_2}{(R - R_m)} - \lambda_v \frac{RR_m(T_s - T_m) - R_m a_2}{(R - R_m)} \right). \tag{2.34}$$

Recalling Eqs. (2.4) and (2.5b), and substituting the value of $v_v|_{r=R}$ from above equation, it is finally obtained that

$$\begin{aligned}\rho_{v_s} L\dot{R} = {} & \lambda_v \frac{R_m(T_m - T_s) - a_2}{R(R - R_m)} + \frac{\sigma R_m^2 (T_m^4 - T_s^4)}{\frac{R^2}{\varepsilon_m} + R_m^2\left(\frac{1-\varepsilon_l}{\varepsilon_l}\right)} - \frac{2\lambda_l (T_s - T_\infty)}{\delta} \\ & + \frac{\rho_{v_s} R_g L}{pC_p R^2}\left(\lambda_v \frac{RR_m(T_s - T_m) + Ra_2}{(R - R_m)} \right. \\ & \left. - \lambda_v \frac{RR_m(T_s - T_m) - R_m a_2}{(R - R_m)} \right).\end{aligned} \tag{2.35}$$

On the right-hand side of the above equation, the last term within parentheses evolves as a result of variable density. The condition for which variable density effects are important are discussed in Appendix A.

The expression for J now takes the form

$$\begin{aligned} J &= \rho_{v_s}(\dot{R} - v_v|_{r=R}) \\ &= \rho_{v_s}\left(\dot{R} - \frac{R_g}{pC_p R^2}\left(\lambda_v \frac{RR_m(T_s - T_m) + Ra_2}{(R - R_m)} \right.\right. \\ &\quad \left.\left. - \lambda_v \frac{RR_m(T_s - T_m) - R_m a_2}{(R - R_m)} \right) \right). \end{aligned} \tag{2.36}$$

The above equation for J is different from that given by Bejan et al. [17], where the velocity field induced by the thermal expansion of the vapour was considered only in the vapour phase of the energy equation and not in the interface mass balance.

Substituting Eq. (2.36) in Eq. (2.10) one gets the liquid-phase energy equation as

$$\begin{aligned} & \left\{ \frac{1}{3} + \frac{1}{3}\left(\frac{\delta}{R}\right) + \frac{1}{10}\left(\frac{\delta}{R}\right)^2 \right\}\dot{\delta} + \left\{ \frac{2}{3}\left(\frac{\delta}{R}\right) + \frac{1}{6}\left(\frac{\delta}{R}\right)^2 + \frac{\rho_{v_s}}{\rho_l} \right\}\dot{R} \\ &= \frac{2\alpha_l}{\delta} + \frac{\rho_v}{\rho_l} \cdot \frac{R_g}{pC_p R^2}\left(\lambda_v \frac{RR_m(T_s - T_m) + Ra_2}{(R - R_m)} \right. \\ &\quad \left. - \lambda_v \frac{RR_m(T_s - T_m) - R_m a_2}{(R - R_m)} \right). \end{aligned} \tag{2.37}$$

Now the continuity equation is written as

$$\frac{\partial}{\partial t}\left(r^2 \rho_v\right) = -\frac{\partial}{\partial r}\left(r^2 \rho_v v_v\right). \tag{2.38}$$

Applying Leibnitz theorem and integrating the above equation from R_m to R, one obtains

$$\frac{d}{dt}\int_R^{R_m} r^2 \rho_v \, dr - R^2 \rho_{v_s} \dot{R} = \left(-r^2 \rho_v v_v\right)\big|_{r=R} + \left(r^2 \rho_v v_v\right)\big|_{r=R_m}. \tag{2.39}$$

Expressing density by $p/R_g T_v$ and noting that $v_v|_{r=R_m} = 0$, the above equation takes the form

$$\frac{p}{R_g}\frac{d}{dt}\int_{R_m}^{R} \frac{r^2 \, dr}{T_v} - \frac{R^2 p}{R_g T_s}\dot{R} = -R^2 \frac{p}{R_g T_s} v_v\bigg|_{r=R}. \tag{2.40}$$

Substitution of the value of $v_v|_{r=R}$ from Eq. (2.34) into Eq. (2.40) yields

$$\begin{aligned} & \frac{p}{R_g}\frac{d}{dt}\int_{R_m}^{R} \frac{r^2 \, dr}{T_v} - \frac{R^2 p}{R_g T_s}\dot{R} \\ &= -\frac{1}{C_p T_s}\left(\lambda_v \frac{RR_m(T_s - T_m) + Ra_2}{(R - R_m)} \right. \\ &\quad \left. - \lambda_v \frac{RR_m(T_s - T_m) - R_m a_2}{(R - R_m)} \right). \end{aligned} \tag{2.41}$$

Using Eq. (2.15e), the above can be expressed as

$$\frac{d}{dt}\int_0^1 \frac{[R_m+\eta(R-R_m)]^3(R-R_m)\,d\eta}{u(\eta)} - \frac{R^2}{T_s}\dot{R} = -\frac{R_g}{pC_pT_s}\left(\lambda_v \frac{RR_m(T_s-T_m)+Ra_2}{(R-R_m)} - \lambda_v \frac{RR_m(T_s-T_m)-R_ma_2}{(R-R_m)}\right). \quad (2.42)$$

The above expression can be rewritten as

$$A\dot{R} + B\dot{a}_2 = -\frac{R_g}{pC_pT_s}\left[\lambda_v \frac{RR_m(T_s-T_m)+Ra_2}{(R-R_m)} - \lambda_v \frac{RR_m(T_s-T_m)-R_ma_2}{(R-R_m)}\right], \quad (2.43)$$

where

$$A = \int_0^1 f(\eta)\,d\eta - \frac{R^2}{T_s}, \qquad B = \int_0^1 g(\eta)\,d\eta,$$

$$f(\eta) = \Big(\big[\{u_m + (u_s-u_m-a_2)\eta + a_2\eta^2\}\{R_m+\eta(R-R_m)\}\big]^2 \times \{R_m+4\eta(R-R_m)\} - (R-R_m)\{R_m+\eta(R-R_m)\}^3T_s\eta\Big) \Big/ \big[u_m+(u_s-u_m-a_2)\eta+a_2\eta^2\big]^2$$

and

$$g(\eta) = \frac{[\{R_m+\eta(R-R_m)\}^3(R-R_m)(\eta+\eta^2)]}{[u_m+(u_s-u_m-a_2)\eta+a_2\eta^2]^2}.$$

A and B in Eq. (2.43) can be computed by numerical integration.

3. Results and discussions

A constant-density analysis has been accomplished by simultaneously solving the three non-linear ODEs given by Eqs. (2.13), (2.16) and (2.17) by fourth-order Runge–Kutta method. To account for the variable-density effects, the same technique has been used for solving Eqs. (2.35), (2.37) and (2.43). The solution provides the temporal variation of δ, a_2 and R corresponding to the initial conditions imposed. It may be noted that from the above solutions, the temperature variation with time can also be extracted.

First, the bubble growth in a superheated liquid has been considered for validation of the constant-density model, since analytical solution under such condition is available [21]. Also, the problem of a collapsing bubble in subcooled liquid has been taken up for comparison with experimental results [22]. Following the model described by Fig. 1, a very small metal sphere of 0.005 mm diameter was considered for validation by simulating both the growth and collapse problems of the vapour bubble, keeping the surface temperature of the interior sphere constant at saturation condition corresponding to the normal atmospheric pressure.

Next, the results obtained on the basis of the constant-density integral formulation have been validated against the incompressible VOF predictions [19]. It has been found for certain values of liquid subcooling and sphere temperatures, the film growth period is preceded by a decay of the film thickness, representing a non-monotonic dynamics. The prediction of the duration of the collapsing period from the simple scale-model analysis has then been compared with the predictions of both the constant and variable-density integral formulations.

Finally, the effects of density variation and radiation on growth of a vapour film over a high temperature sphere of larger sizes by mass transfer from an infinite expanse of water has been studied. The effect of vapour-phase density variation has been analysed and compared with the constant-density predictions, incorporating vapour-phase radiation in both the models. It is to be noted that the variable-density model in the present work considers the effects of conduction, convection and radiation within the vapour film along with the effect of convection in the interfacial mass and energy balance. The variable density model has been extensively used to investigate the effects of different initial thickness of the film, liquid subcooling, sphere temperature and sizes.

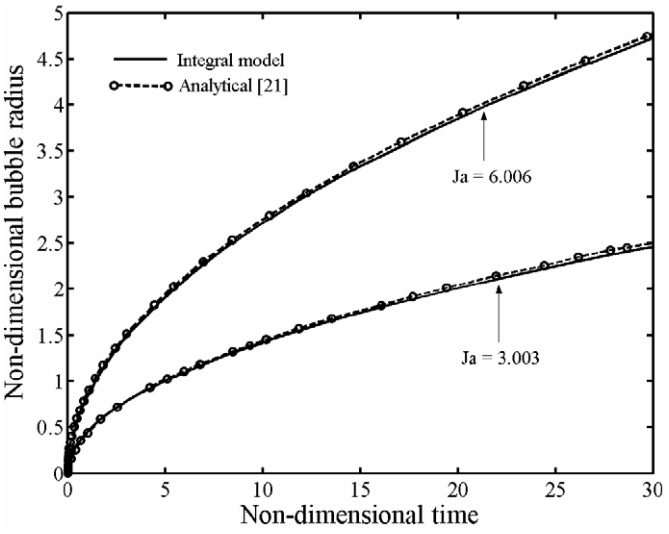

Fig. 2. Transient growth of a vapour bubble in superheated liquid.

3.1. Validation of the constant density model

3.1.1. Spherical growth of a bubble in a superheated liquid

The thermally driven bubble growth in a superheated water layer of infinite expanse at atmospheric pressure is considered here. Son [21] obtained the analytical solution by neglecting the vapour compressibility and the dynamic effect of liquid inertia. Under these assumptions, surface tension balances the bubble internal pressure, p_{int} (that can be obtained by solving Laplace equation as $p_{\text{int}} = p_\infty + 2\gamma/R$) and the bubble growth is sustained only by evaporation. Two different Jakob numbers (Ja) of 3.003 and 6.006 were considered corresponding to liquid–vapour density ratio of 1603 and water superheat of 1 and 2 K, respectively. The length scale was arbitrarily set as 0.5 mm and the velocity and time scales as $(gR)^{1/2}$ and $(R/g)^{1/2}$, respectively [21]. For validation of the integral model with the analytical solution, initial bubble radius and liquid-side thermal layer thickness were assumed to be 0.008 and 0.005 mm, respectively. The temperature of the sphere was kept constant by specifying it at saturation temperature of 100 °C corresponding to atmospheric pressure, while the far stream was considered as maintained at the specified superheated temperature. Fig. 2 reveals an excellent agreement of the bubble growth simulated by the integral model against the analytical solutions.

3.1.2. Collapse of vapour bubble in subcooled liquid

Another validation of the integral model has been undertaken against the experimental results of collapsing and slowly translating steam bubble by Florschuetz and Chao [22], as reported by Riznic et al. [8]. Corresponding to this experiment, a Jakob number of 39.3 and an initial bubble radius of 3.67 mm were considered for the validation. An initial thermal layer thickness of 0.01 mm was chosen in the integral model. As observed from Fig. 3, up to a non-dimensional time ($4Ja^2\alpha_l t/\pi R_0^2$) of 0.4, the transient bubble

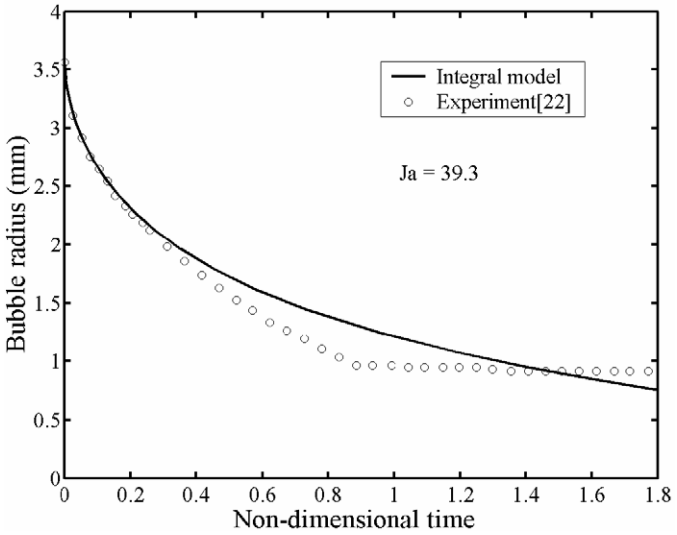

Fig. 3. Collapse of a vapour bubble in subcooled liquid.

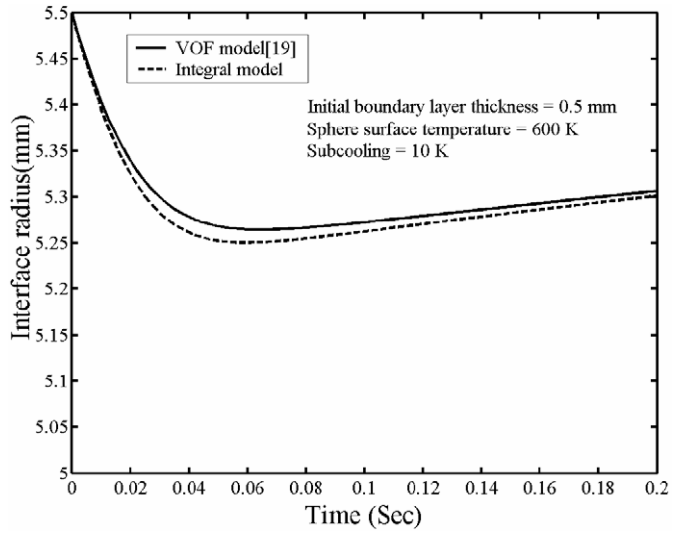

Fig. 4. Comparison of VOF and integral models.

radius matches well with the integral model. The observed discrepancy beyond this time might be due to the presence of some non-condensable gas and small translation motion not considered in the integral model. Riznic et al. [8] reported similar deviations in the context of integral analysis.

3.1.3. Comparison of predictions from VOF and integral models

A validation of the constant-density integral model is presented here through a comparison with a more rigorous incompressible VOF-based formulation [19] in terms of the time variation of liquid–vapour interface radius in Fig. 4. For comparison with the VOF model developed, the effect of radiation has been omitted for validation in the results of the integral model presented in Fig. 4. A sphere of 5 mm diameter at 600 K has been considered with a vapour film on it that has initial thickness of 0.5 mm, the film being surrounded by water subcooled by 10 K. The initial thermal layer thickness of 0.5 mm in the liquid side has been considered. At the interface, both models predict an initial period of rapid condensation leading to faster collapse in comparison to the subsequent growth period that is due to evaporation. The integral model shows the interface radius to reduce to a minimum of 5.25 mm at 62.69 ms, whereas the VOF predictions of these

Table 1
Comparison of computational run time of VOF-model and Integral model.

Liquid boundary layer thickness (mm)*	Computational run time (min) (VOF-based model)
0.5	6
0.2	9
0.1	30
0.01	150

* In all the above cases, the integral model required a few seconds (∼ 4–5 s) of computation time, which was practically insensitive to choices of initial liquid layer thickness.

values are 5.26 mm at 60.25 ms. Following the collapse, the contribution of diffusive heat transfer is predominant over liquid side heat transfer and both models show an expected trend of growth.

It may be mentioned here that on a Pentium IV computer with 2.66 GHz processor, the VOF simulation of the above problem takes about 6 minutes to complete one typical run for initial value of liquid thermal layer of 0.5 mm, whereas the integral model returns the result in a few seconds. The several-order gain in speed of computation without much sacrifice in accuracy makes the integral model extremely suitable for a system level study that needs addressing the interaction among multiple particles. The computational economy of the integral model is further evident from the fact that while the time taken by the VOF model increases steeply with decrease in initial thickness of the liquid thermal layer, the computation time of the integral model is practically unaffected. Some representative computation times are shown in Table 1. We would also like to mention here that computation times for both the integral models, using constant density and variable density formulations are similar. Apart from the need of extremely refined grid for investigating dynamics when the initial vapour-phase thickness or the liquid-side boundary layer thickness is very small, the other limitations of the VOF formulation are the difficulties of integrating the radiation and variable density effects. In order to validate the integral model predictions corresponding to negligible values of the thickness of both the initial film and the thermal layer, a scale analysis has been carried out.

3.2. Comparison of constant and variable density models with scale model predictions

The results from scale analysis and integral model are considered in this section. The initial conditions have been taken as in the preceding section except for the initial liquid-side thermal boundary layer thickness. A negligibly small value of 0.0005 mm has been chosen here as the thermal layer thickness. This is done in order to compare the integral model results with that of the scale analysis that assumes the initial thermal layer thickness as zero, as can be seen in Eq. (2.21). Fig. 5 exhibits that the predictions of the initial collapse period by the order-of-magnitude scale model and the constant-density integral model are in reasonable agreement up to the rebound time as predicted by Eq. (2.26a) pertaining to the scale analysis. The rebound time obtained from Eq. (2.26a) and the integral model are 1.789 and 1.56 ms, respectively. Fig. 5 also traces the rapid degradation of the scale-model prediction beyond the rebound time.

For melt surface temperature of 600 K and bulk-liquid subcooling of 10 and 20 K, it has been obtained that the rebound time predictions are 1.560 and 0.406 ms, respectively, from the scale analysis and 2.100 and 0.440 ms, respectively, from the constant-density model. As the effect of liquid side heat transfer increasingly dominates at higher subcooling during the collapsing phase, the scale analysis, which neglects vapour side heat transfer, clearly gives better agreement.

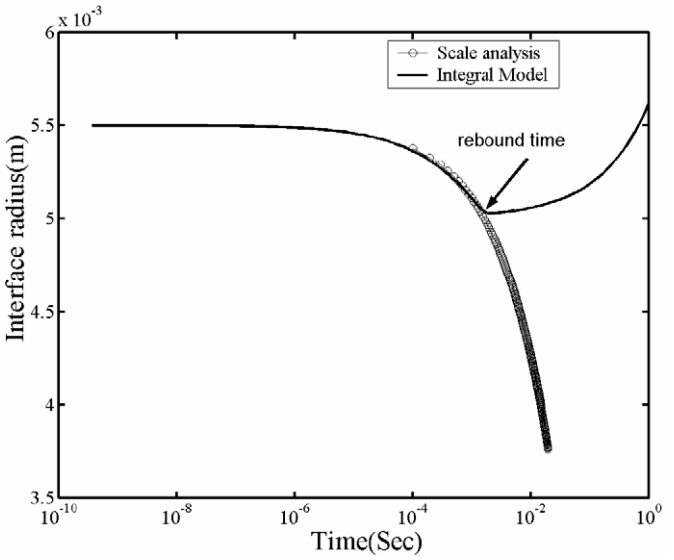

Fig. 5. Comparison of scale analysis and integral results for sphere temperature of 600 K at 10 K liquid subcooling.

3.3. Effects of density variation and radiation

3.3.1. Growth of vapour film in superheated liquid

The incompressible VOF-based solution [19] of spherico-symmetric growth of a liquid–vapour phase front has been used here to validate the variable-density model developed here in the limit of constant density. Spheres of radii 5 and 50 mm with an initial vapour-phase thickness of 1 mm in each case were chosen. The surface of the sphere was assigned a saturation temperature of water at 1 atmospheric pressure. For this configuration, referred to as "sucking problem" by Welch and Wilson [13], it may be noted that the vapour film remains at saturation temperature at all times. Hence no thermally induced velocity field is generated. An initial boundary layer thickness of 0.5 mm was considered in the liquid side with a superheating of 5 K. Fig. 6a compares the predicted increase in film thickness for the two sphere sizes, as obtained from the VOF and integral models. The present model shows excellent agreement with the VOF-based code. Fig. 6b depicts a similar agreement between the predictions of the two models for the temperature profile at 2.5 sec.

3.3.2. Role of vapour-phase density variation in interface modeling

The effects of vapour-phase density variation and radiation on liquid–vapour interfacial growth have been studied here to assess the effect of density variation in interface energy balance. Bejan et al. [17] formulated the energy equation assuming it as ideal gas and considering radiation and motion of vapour phase without, however, incorporating the last effect in the interfacial energy. Eq. (2.35) of the present model has thus been rewritten for a saturated liquid by excluding the effect of vapour-phase density variation to obtain that

$$\rho_{v_s} L\dot{R} = \lambda_v \frac{R_m(T_m - T_s) - a_2}{R(R - R_m)} + \frac{\sigma R_m^2 (T_m^4 - T_s^4)}{\frac{R^2}{\varepsilon_m} + R_m^2\left(\frac{1-\varepsilon_l}{\varepsilon_l}\right)}. \tag{3.1}$$

The above equation is identical with Eq. (15) of [17]. A hot sphere of 1 mm radius at 2295 K has been considered along with a very thin vapour film thickness of 0.001 mm. The emissivity of 0.8 is considered both for sphere surface and water-steam interface. The growth of liquid–vapour interface with time is shown in Fig. 7. The results of Fig. 7 show that the predictions of the present model using Eq. (3.1) for evaluation of $\dot{R}$, deviate from the predictions of Bejan et al. [17] by a maximum of about 1%. The same

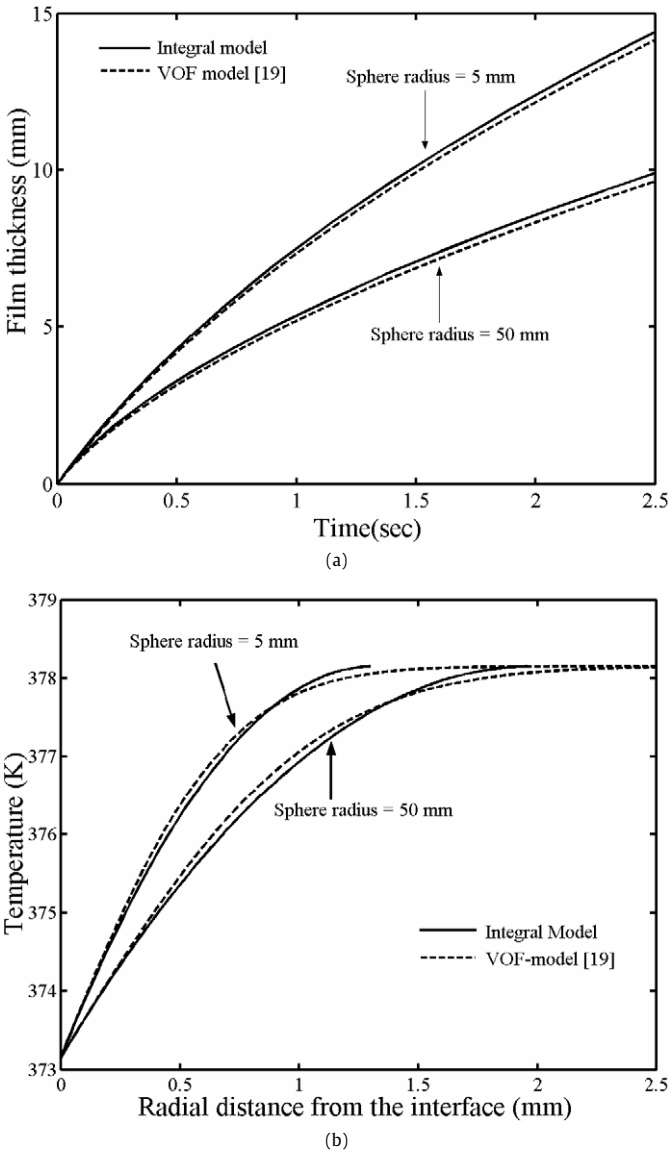

Fig. 6. Comparison with respect to the sucking problem for (a) transient growth of film, and (b) temperature variation within liquid at 2.5 sec.

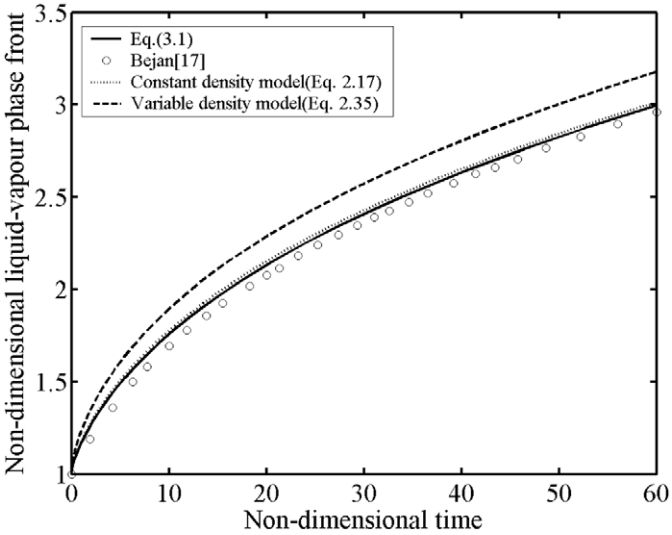

Fig. 7. Effects of vapour phase and interface modeling on predicted growth of liquid–vapour phase front.

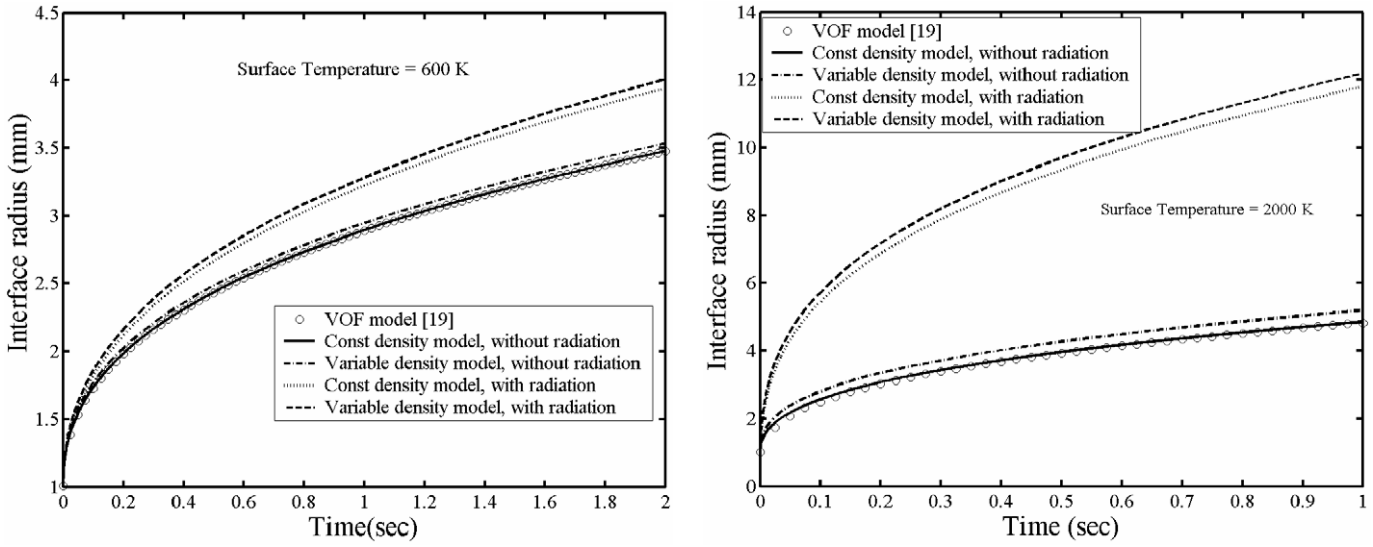

(a) (b)

Fig. 8. Comparison of constant density and variable density models for surface temperature (a) 600 K and (b) 2000 K.

figure also shows the predictions for constant density and variable density models using Eqs. (2.17) and (2.35), respectively. The latter considers the convective effects in both the vapour phase energy equation and interface mass balance.

The growth rate of the film is seen to be significantly affected by the vapour velocity at the interface. Thermal expansion of the vapour phase gives rise to a dilatational velocity at the interface that causes radial advancement of the interface in addition to that caused by the evaporation. Eq. (2.35) considers both these effects, while Eq. (3.1) does not consider the first one. Consequently, the value of $\dot{R}$ is significantly under-predicted by Eq. (3.1). The results show significant deviation in the three predictions, highlighting the importance of using Eq. (2.35) instead of Eq. (3.1), especially at high temperatures.

3.3.3. Effects of vapour-phase density variation and radiation on growth of a vapour film in saturated liquid

In this section, the effect of variation of density and radiative heat transfer has been studied in terms of results from both constant and variable-density integral models and from models with and without radiation. It may be noted that both of the effects under study become significant at high temperatures. Therefore, the cases of a sphere at temperatures equal to 600 and 2000 K have been considered for which the growth predicted in terms of the liquid–vapour interface radius in saturated water has been predicted in Figs. 8a and 8b, respectively, up to 2 and 1 s. An initial film thickness of 0.5 mm on the sphere of 5 mm diameter has been studied. The effect of density variation has been considered both in the vapour film energy equation and the interfacial energy balance.

It can be seen from both Figs. 8a and 8b that the predictions of the constant-density integral model without radiation are in excellent agreement with the results of the incompressible VOF-based study [19] that does not consider radiation. The predictions of the interface radius in these figures have been compared under two situations for the assessment of the effects of radiation and vapour-phase density. While Case 1 corresponds to 600 K sphere temperature after 2 s, Case 2 corresponds to 2000 K sphere temperature after 1 s. In absence of radiation, the variable-density model predictions for Cases 1 and 2 are, respectively, 1.8 and 3.3% more than those of the constant-density model. However, the effect of radiation on film growth on the basis of variable-density model predictions is observed to be far more pronounced. The predictions of the interface radius are seen to increase by 15 and 140%, respectively, for Cases 1 and 2, respectively, when the results without radiation are compared with results taking radiation into account.

3.4. Parametric study

In this section, a parametric study has been performed with the variable density and radiation model. The film collapse and growth for different parameters, namely the film thickness, degree of subcooling, sphere surface temperature, sphere size are presented. It is interesting to note that our integral model is capable of predicting the non-monotonous dynamics of the film collapse and growth.

Fig. 9a shows the film collapse and growth for different initial film thickness. It is found that lower the initial film thickness, smaller the rebound time and the corresponding film thickness are. The rebound times are 6.64, 1.50, 0.21 and 0.05432 ms for initial film thickness of 1, 0.5, 0.2 and 0.1 mm, respectively. The corresponding film thicknesses are seen to be 0.1953, 0.076, 0.0262 and 0.0126 mm, respectively. Fig. 9a shows that although the collapsing rate depends on film thickness, the subsequent diffusion induced growth are observed to be similar.

Fig. 9b shows the collapse and growth for different subcooling in liquid for a sphere size of 5 mm and sphere surface temperature of 1000 K. While the zero subcooling shows the asymptotic growth of interface, the cases with progressively higher subcooling show progressively faster collapse with lowering of duration of collapsing period, as shown in the figure. The collapsing times for 5, 10 and 20 K subcooling are 2.9, 1.55, and 0.345 ms, respectively. The corresponding interface radii are 5.262, 5.076 and 5.017 mm, respectively. In this case the growth after the collapse phases are observed to be more for less bulk subcooling level.

The variation of surface temperature of the sphere on film collapse and growth is presented in Fig. 10a. The sphere with higher surface temperature shows faster collapse, but at a higher interface thickness. The collapsing time for various sphere surface temperature of 600, 1000, 1500 and 2000 K are 0.275, 1.1, 1.6 and 1.8 ms, respectively. The corresponding interface radii are 5.385, 5.21, 5.07 and 5.025 mm, respectively. The subsequent larger growth of film thickness for higher temperature is expected due to pronounced effect of radiation at high temperature. It is to be

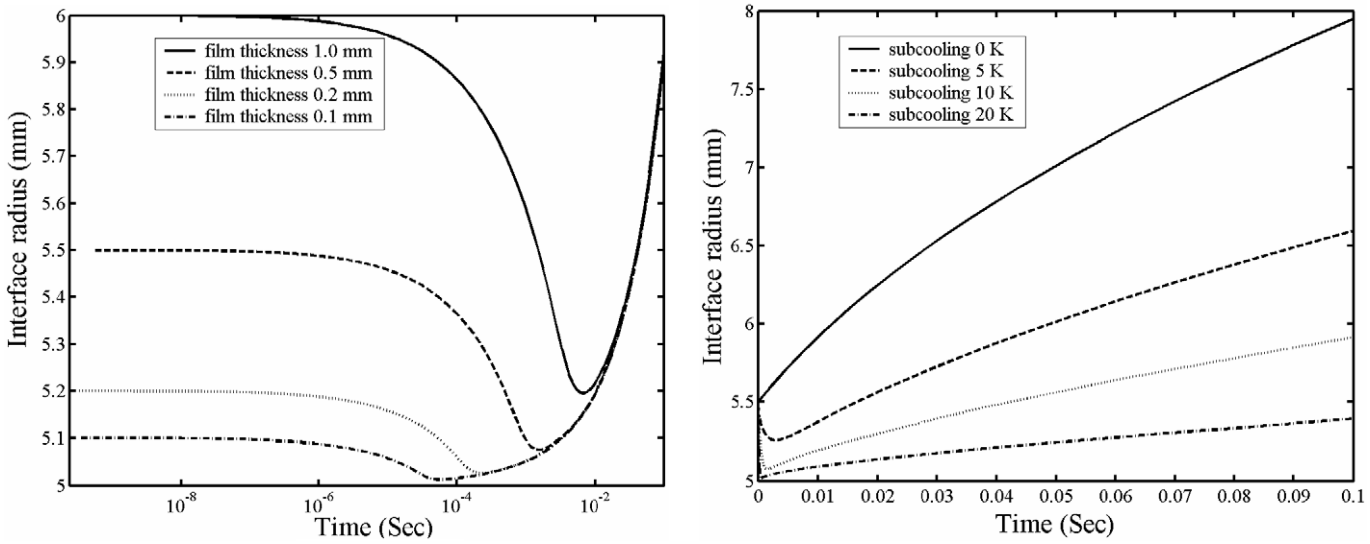

(a) (b)

Fig. 9. Transient collapse and growth of liquid–vapour interface for different (a) initial film thickness, and (b) degrees of subcooling.

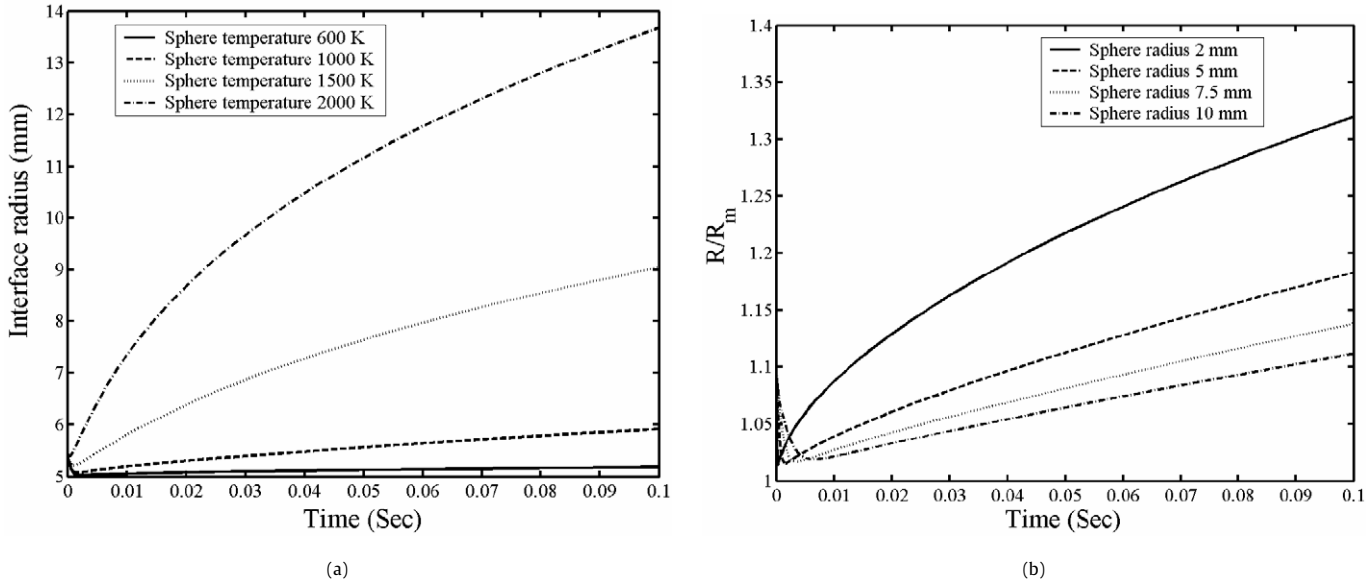

(a) (b)

Fig. 10. Transient collapse and growth of liquid–vapour interface for different (a) sphere temperatures, and (b) sphere sizes.

noted that at lower surface temperature at 600 K, the growth is very small.

Transient collapse and growth for different values of sphere radius are considered next. An initial film thickness of 10% of the sphere radius was assumed. The rebound time for 10, 7.5, 5.0 and 2.0 mm sphere sizes are 6.5, 3.5, 1.5 and 2.4 ms, respectively. The corresponding interface radius to sphere radius ratio (R/R_m) are 1.019, 1.0619, 1.015 and 1.0136, respectively. One with lower sphere size shows the faster collapse and growth as shown in Fig. 10b.

4. Conclusions

Two integral models have been developed for simulating spherico-symmetric liquid–vapour phase-change with two immiscible phases. In one model the density variation within the film was neglected while it was included in another model with an ideal gas approximation. The effect of motion was included both in film energy balance and interfacial mass and energy balance. Both models were validated with some known solutions. Finally, both the models were compared with and without the consideration of radiation. It is observed that both density variation and radiation within the vapour have influence, particularly at high surface temperatures. Both models take a very low run time and therefore can be easily interfaced in a system level study with multiple spheres. The duration of the collapsing period was derived from a scale model and compared with integral model. It is observed from scale analysis that the initial collapse is primarily governed by Jakob number in liquid side, while the collapsing time is found to dependent on Stefan number in the vapour film side and Jakob number in the liquid side. Finally parametric variation for different initial film thickness, degree of subcooling, sphere surface temperature and sphere radii were presented. It is observed that one with lower thickness shows faster collapse, but subsequent film growth is observed to be similar for same subcooling. The effect of subcooling increases the collapse rate with a subsequent retarded growth. With increase in sphere surface temperature, the collapsing time is lower with a subsequent higher film growth. Finally the lower sphere size shows a faster collapse and growth.

Appendix A

For variable density effects to be important at the interface, $v_v|_R \ll \dot{R}$. Neglecting subcooling and radiation effects, from Eqs. (2.5b) and (2.33),

$$\dot{R} = -\frac{\lambda_v}{\rho_{v_s} L}\left.\frac{\partial T_v}{\partial r}\right|_R$$

and

$$v_v|_R = \frac{\lambda_v}{\rho_{v_s} C_p T_s}\left(\left.\frac{\partial T_v}{\partial r}\right|_R - \frac{R_m^2}{R^2}\left.\frac{\partial T_v}{\partial r}\right|_{R_m}\right).$$

Hence the condition for negligible variable density effect reduces to

$$\left.\frac{\partial T_v}{\partial r}\right|_R \left(1 + \frac{C_p T_s}{L}\right) \ll \frac{R_m^2}{R^2}\left.\frac{\partial T_v}{\partial r}\right|_{R_m}.$$

Assuming that $(R - R_m)/R_m \ll 1$, which is true for a significant extent of time, the curvature effect can be neglected and the temperature gradients can be adopted from the exact solution of one-dimensional planar Stefan problem [23]. The temperature gradients are

$$\left.\frac{\partial T_v}{\partial r}\right|_R = -\frac{T_m - T_s}{erf(\lambda)}\frac{1}{(\alpha_v t)^{1/2}\sqrt{\pi}}\exp(-\lambda^2),$$

$$\left.\frac{\partial T_v}{\partial r}\right|_{R_m} = -\frac{T_m - T_s}{erf(\lambda)}\frac{1}{(\alpha_v t)^{1/2}\sqrt{\pi}}.$$

In the above equation, $\lambda = (R - R_m)/2(\alpha_v t)^{1/2}$is a function of Stefan number *Ste*.

The values of λ for different Stefan numbers are given in Table 11-2 of [23].

Substituting the expression for temperature gradients, the condition for neglecting variable density effects becomes

$$\frac{R}{R_m} \ll \left[\left(1 + \frac{C_p T_s}{L}\right)\exp(-\lambda^2)\right]^{-1/2}.$$

For typical values of Stefan number considered in the problem ($(T_m - T_s) \sim$ 300–2000 K), $\lambda \sim 0.5$–1.0. For this range of λ, the condition becomes $R/R_m \ll O(1)$. Since $R/R_m \geqslant 1$, this implied that variable density effects are always important for the situations considered.

References

[1] M.S. Plesset, S.A. Zwick, The growth of vapour bubble in superheated liquid, J. Appl. Phys. 25 (1954) 493.
[2] B.B. Mikic, W.M. Rosenhow, P. Griffith, On bubble growth rates, Int. J. Heat Mass Transfer 13 (1970) 657–666.
[3] M. Dalle Donne, M.P. Ferranti, The growth of vapor bubble in superheated Sodium, Int. J. Heat Mass Transfer 18 (1975) 477–493.
[4] A. Prosperetti, M.S. Plesset, Vapour-bubble growth in a superheated liquid, J. Fluid Mech. 85 (1978) 349–368.
[5] H.S. Lee, H. Merte Jr., Spherical vapor bubble growth in uniformly superheated liquids, Int. J. Heat Mass Transfer 39 (1996) 2427–2447.
[6] A.J. Robinson, R.L. Judd, The dynamics of spherical bubble growth, Int. J. Heat Mass Transfer 47 (2004) 5101–5113.
[7] J. Naude, F. Mendez, Numerical analysis of an asymptotic model for the collapse of a vapor bubble, Heat and Mass Transfer 43 (4) (2007) 325–331.
[8] J. Riznic, G. Kojasoy, N. Zuber, On the spherically symmetric phase change problems, Int. J. Fluid Mechanics Research 26 (2) (1999) 110–145.
[9] A.A. Avdeev, Y.B. Zudin, Inertial-thermal governed vapor bubble growth in highly superheated liquid, Heat Mass Transfer (2005) 855–863.
[10] B. Sarler, Stefan's work on solid–liquid phase changes, Engineering Analysis with Boundary Elements 16 (1995) 83–92.
[11] J. Caldwell, Y.Y. Kwan, On the perturbation method for the Stefan problem with time-dependent boundary conditions, Int. J. Heat Mass Transfer 46 (2003) 1497–1501.
[12] H.S. Carslaw, J.C. Jaeger, Conduction of Heat in Solid, Oxford University Press, London, 1967.
[13] S.W.J. Welch, J. Wilson, A volume of fluid based method for fluid flows with phase change, J. Comp. Phys. 160 (2000) 662–682.
[14] A. Esmaeeli, G. Tryggvasson, Computations of film boiling, Part I. Numerical methods, Int. J. Heat Mass Transfer 47 (2004) 5451–5461.
[15] D.F. Fletcher, Steam explosion triggering: a review of theoretical and experimental investigations, Nuclear Engrg. Design 155 (1995) 27–36.
[16] G. Berthoud, Vapor explosions, Ann. Rev. Fluid Mech. 322 (2000) 573–611.
[17] A. Bejan, N. Dan, D.G. Cacuci, W. Schutz, On the thermodynamic efficiency of energy conversion during the expansion of a mixture of hot particles, steam and liquid water, Energy 22 (12) (1997) 1119–1133.
[18] N. Dan, A. Bejan, D.G. Cacuci, W. Schutz, Evolution of a mixture of hot particles, steam and water immersed in a water pool, Numer. Heat Transfer A 34 (1998) 463–478.
[19] K. Ghosh, A. Mukhopadhyay, S. Sen, D. Sanyal, A spherico-symmetric VOF approach for investigating immiscible two-phase systems with one liquid phase, Numerical Heat Transfer A 50 (2006) 949–974.
[20] O. Craciunescu, A. Bejan, D.G. Cacuci, W. Schutz, Time-dependent interaction between water at supercritical pressures and a hot surface, Numerical Heat Transfer A 30 (1996) 535–553.
[21] G. Son, A numerical method for bubble motion with phase change, Numerical Heat Transfer B 39 (2001) 509–523.
[22] L.W. Florschuetz, B.T. Chao, On the mechanics of vapor bubble collapse, J. Heat Transfer 87 (1965) 209–220.
[23] M.N. Ozisik, Heat Conduction, John Wiley and Sons, 1967.